Current Research in Food Science 12 (2026) 101374

Contents lists available at ScienceDirect

Current Research in Food Science

journal homepage: www.sciencedirect.com/journal/current-research-in-food-science

Detection and identification of insect processed animal proteins in microscopic images using deep learning

Cyril Kaisin [b], Pascal Veys [a,*], Abigaël Anselmo [a], Bernard Gosselin [b]

[a] Knowledge and Valorisation of agricultural Products Department, Walloon Agricultural Research Centre, Chaussée de Namur 24, Gembloux, 5030, Belgium
[b] ISIA Lab, Faculty of Engineering, University of Mons, Boulevard Dolez 31, Mons, 7000, Belgium

ARTICLE INFO

Handling Editor: Professor Georgios Leontidis

Keywords:
Deep learning
Microscopy
Insect meal
Feed
Processed animal proteins

ABSTRACT

The introduction of terrestrial invertebrate processed animal proteins (PAPs) from insects in animal feed has introduced challenges for official controls in the European Union. Currently, their detection relies only on light microscopy and is entirely dependent on the expertise of trained operators. Recent studies have highlighted two primary problems regarding insect PAP detection: specificity issues due to the misidentification of non-insect structures as insect derived ones, and the difficulty in categorizing a wide morphological diversity of particles resulting from the grinding of whole insect larvae. To address these limitations, a proof of concept was developed involving automated microscopic image analysis and classification by deep learning. A classification pipeline integrating a YOLO object detection model with an improved ConvNeXt architecture coupled with transformer blocks was tested. After supervised learning, training and validation of the model, obtained results allowed to successfully distinguish insect particles from other non-insect materials, and to discriminate PAPs particles derived from *Tenebrio molitor* and *Hermetia illucens* achieving average Matthews Correlation Coefficient of 0.89 and accuracies exceeding 95% for both tasks. The robust performance and the rapid processing speed of the model enabled to couple it to a digital microscope for real-time automated particle classification, including confidence scores for individual particle predictions. This artificial intelligence model for microscopic identification of complex structures opens new perspectives for official controls achieving performance scores never reached before. It provides to microscopists an optimisation of image analysis and a valuable decision-support tool in complex feed matrices where human expertise is frequently challenged.

1. Introduction

Insect-derived meals represent a sustainable and valuable alternative protein source for both direct human consumption and animal feeding, as promoted for years by the Food and Agriculture Organization of the United Nations (FAO, 2013). The use of insects, either whole or as processed animal proteins (PAPs), was first legally introduced in the European Union (EU) in 2017 for aquaculture feed (European Commission, 2017). This authorisation was later extended in 2021 to the feeding of pig, poultry, pet and fur animals (European Commission, 2021a), while their utilisation remains prohibited for ruminant and other non-ruminant animals.

Currently, only eight insect species are approved and considered as farmed insects under EU legislation (European Commission, 2017, 2021b): the black soldier fly (*Hermetia illucens*), the common housefly (*Musca domestica*), the yellow mealworm (*Tenebrio molitor*), the lesser mealworm (*Alphitobius diaperinus*), the house cricket (*Acheta domesticus*), the banded cricket (*Gryllodes sigillatus*), the field cricket (*Gryllus assimilis*) and the silkworm (*Bombyx mori*). Of these, only two species, *H. illucens* and *T. molitor,* are the most predominantly reared for PAP production and commercialisation. The transformation of the insect larvae into PAPs occurs through several processing steps including blanching, grinding, drying and mixing to yield high proteinic meals suitable to be introduced in compound feed formulations (Rossi et al., 2025). Consequently, these processing steps often imply a loss of the visual characterisation enabling to identify the insect origin of the meals.

Given regulatory constraints, such as their prohibition for ruminants, and the closed list of authorised insect species, efficient analytical methods are needed to support official controls to prevent feed frauds or cross contaminations and ensure compliance. Insect meals, as PAPs, fall in the EU under the scope of regulation EC/152/2009 (European

* Corresponding author.
E-mail address: p.veys@cra.wallonie.be (P. Veys).

https://doi.org/10.1016/j.crfs.2026.101374
Received 24 November 2025; Received in revised form 18 February 2026; Accepted 3 March 2026
Available online 4 March 2026

Commission, 2009) which defines the control methods in its sixth annex.

According to current regulation and the related standard operating procedures issued by the European Reference Laboratory for animal proteins detection in feedingstuffs (EURL-AP, Gembloux, Belgium), the only official method for insect detection in feed is light microscopy following a double sedimentation sample preparation protocol (Veys and Baeten, 2018). This technique is based on the specific densities of insect cuticular fragments to concentrate and better isolate them from complex feed matrices. Light microscopy is a detection method which allows only a qualitative result expression – indicating presence or absence of insect material. This method relies thus entirely on the expertise of trained analysts which introduces subjectivity and variability in performance.

Expertise is precisely the bottleneck at which performance issues struggle. Prior to implementation of the double sedimentation protocol, a collaborative study organised in 2014, involving feed samples spiked with 1% of grasshopper meal, concluded that only 10% out of 52 laboratories succeeded at identifying correctly the presence of insects (van Raamsdonk et al., 2017), highlighting a major sensitivity issue. Since then, the implementation of the double sedimentation, combined with a more frequent exposure of insect meals and access to reference micrographs, have led to substantial gains in insect detection capabilities. Proficiency tests, organised in 2023, demonstrated sensitivity scores up to 84% (Veys and Fumière, 2023), and in some cases of 100% (Veys et al., 2024). Despite these improvements, the same studies showed the emergence of specificity issues. Misidentification of non-insect structures as insect-derived particles has led to false positive results. Specificity issues are primarily due to the large diversity of insect fragments obtained by the grinding of entire larvae or imagos. Insect meals contain cuticular fragments with setae, appendices such as antennae, legs, wing parts, uncharacterised muscle fibres, parts from tracheal respiratory systems, mouth parts, sclerotised and unsclerotised areas such as soft join cuticles, and finally soft tissues from the digestive tract. Even with a strong entomological histological expertise, the identification of such heterogeneous components is challenging. Additionally, some cuticular particles exhibit geometrical structural patterns that mimic plant structures, such as the aleurone layer of wheat (Veys and Fumière, 2021), further increasing the likelihood of false positive misidentifications.

To address these challenges, we explored the use of deep learning for automated microscopic image-based detection and classification of insect particles. Deep learning is a subset of machine learning, defined by advanced capabilities from the use of convolutional neural networks (CNN) after implementing back-propagation to reduce errors and optimize classification predictions, offering both independent learning capabilities and high efficiency of own correct decisions (Zinchuk and Grossenbacher-Zinchuk, 2020). Although well established in biomedical imaging, applications in food and feed microscopy remain relatively limited. Nonetheless, the number of publications applying deep learning in this domain has increased markedly between 2015 and 2022 (Othman et al., 2023). Recent studies have demonstrated its potential for automated detection of foodborne bacteria (Ma et al., 2023; Papa et al., 2025; Park et al., 2023), fungal contamination (Przybył et al., 2020), spores (Li et al., 2023) and microplastics (Bin Zahir Arju et al., 2025).

Unlike prior studies focused on well-defined and uniform objects, the present work explored the feasibility of deep learning for correct classification of morphologically diverse insect particles. The first objective was to select an appropriate supervised model capable of distinguishing insect cuticular particles and to sort them from other non-insect ones. The second aim was to assess the model's ability to discriminate cuticular particles from *T. molitor* and *H. illucens*, a task considered difficult even for experienced microscopists. Finally, the model was coupled to a digital microscope to enable real-time detection of insect particles in compound feeds, providing a practical decision-support tool for official control laboratories where visual identification remains a major analytical challenge.

2. Materials and methods

2.1. Materials

2.1.1. Matrices

The insect PAPs used consisted of two commercially available meals from *H. illucens* and *T. molitor,* intended for animal feeding. These meals were produced from insect larvae and did not contain imagos.

For the development and training of the supervised model, other matrices, recorded within the reference collection of the EURL-AP, were also used. Some of these matrices were generated internally using commercially available compound feed containing plant material (wheat bran, rapeseed, soya, etc.) as well as PAPs from terrestrial vertebrates and feed materials such as fish or krill meal. A sample adulterated with insect meals at a rate of 5 % (w/w) was also used for real-time detection testing. Matrices such as krill or wheat bran were selected because of their morphological patterns resembling insect cuticular structures (Veys and Fumière, 2021). The integration of confounding matrices, or negative examples, helps enhance the discriminative capacity of the deep learning model and reduce false positive classifications (Goodfellow et al., 2016).

All of these samples were subjected to the double sedimentation protocol (Veys and Baeten, 2018) to generate slides from both the sediment and the floating fractions using a 250 μm filter (four slides <250 μm and one slide >250 μm). Microscopic slides from the sediments and floating fractions were prepared according to Annex VI of EC/152/2009 (European Commission, 2009) and related published Standard Operating Procedures (SOPs) (https://www.eurl.craw.eu). Cuticular particles, which constitute the target component of the model and the most abundant components in insect meals, were predominantly recovered in the floating fractions due to their low density.

2.1.2. Micrographs and real-time set-up

Micrographs were acquired using two imaging systems: a digital microscope (Keyence VHX-7000, Osaka, Japan) and an inverted light microscope (Olympus IX83, Tokyo, Japan), both equipped with high-resolution digital sensors. All observations were performed using bright-field illumination under transmitted light. Colour images were captured from slides at magnifications ranging from x200 to x500 with a resolution of 2048 x 1536 pixels.

For real time testing of the model, the Keyence VHX-7000 digital microscope was employed, allowing live visualisation as well as interactive zooming and panning across the slide for detailed examination. The model was executed on a MacBook Air M2 (Apple Inc., Cupertino, USA) with 8 GB of unified RAM connected to the microscope via a smartphone, enabling real-time inference.

2.2. Deep learning

To construct the artificial intelligence (AI) model, three main steps were followed: data preparation, which includes data acquisition (Section 2.1) and preprocessing; model development, where several architectures are trained and evaluated; and finally, model deployment, in which the best-performing model is selected and used for real-time application (Fig. 1).

2.2.1. Raw dataset pre-processing

The large diversity of particles from the micrographs was segmented, masked, and manually annotated by an expert scientist using Labelme v4.6.0 (Wada, 2021). Annotations were first grouped into two classes, “insect” (all insect cuticles) and “non-insect” (all other particles and reference matrices), before further subdividing the “insect” class into *H. illucens* and *T. molitor*. The total labelled dataset included 747 particles of *H. illucens*, 502 particles of *T. molitor*, and 4915 particles from non-insect origin.

Images were normalised by converting them into tensors and

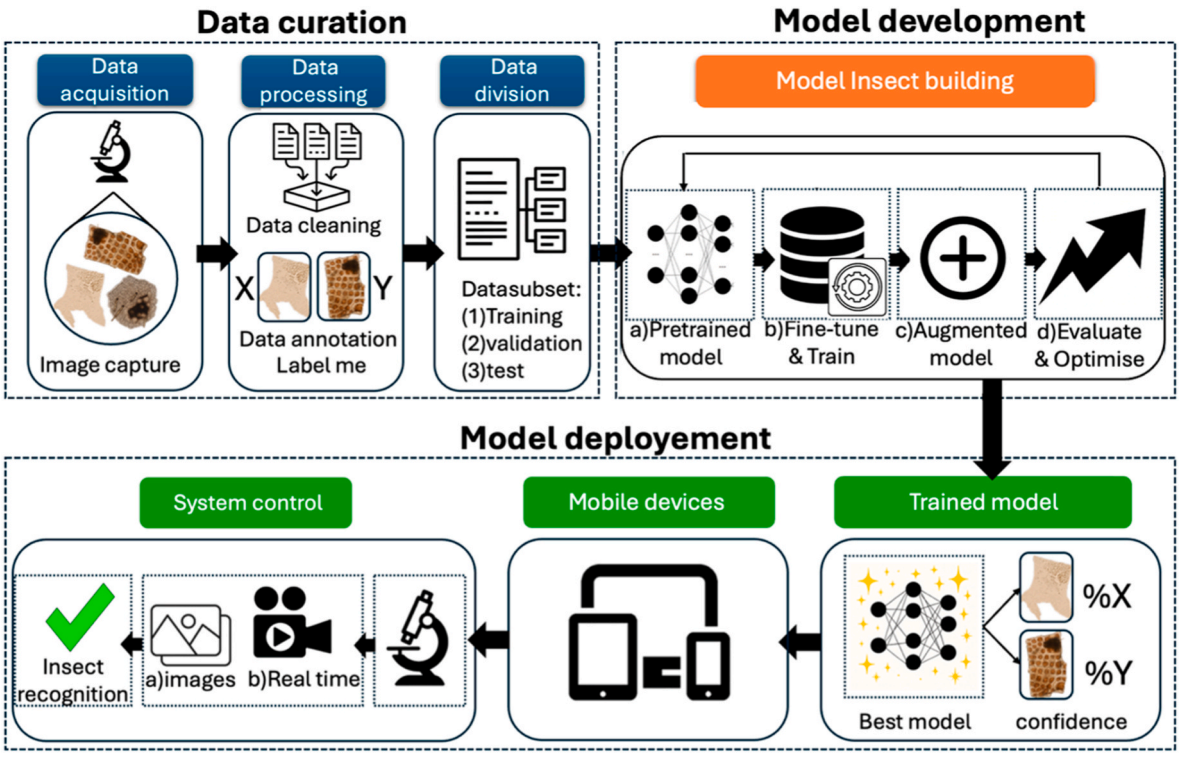

Fig. 1. Schematic representation of the Artificial Intelligence workflow developed for insect particle detection.

rescaling pixel intensities from 0 to 255 to the [0,1] range to ensure efficient training and stable optimisation. All particles, originally sized up to 1500 × 2054 pixels, were resized with individual particles scaled to occupy the full frame. To increase robustness and reduce overfitting, data augmentation was applied through geometric and photometric transformations (rotations, flips, scaling, contrast or colour adjustments) as well as Mixup (Zhang et al., 2017) and CutMix (Yun et al., 2019).

2.2.2. Training strategy model

Several model architectures were initially considered, including Convolutional Neural Networks (CNNs) such as ResNet (He et al., 2016), EfficientNet (Tan and Le, 2019) transformer-based architectures, like Vision Transformer (Dosovitskiy et al., 2021) and Swin Transformer (Liu et al., 2021), and lastly hybrid approaches such as ConViT (d'Ascoli et al., 2022) and CMT (Guo et al., 2022). All models were pretrained on large-scale datasets and fine-tuned using the present dataset. Different model sizes were also tested to evaluate the balance between predictive performance and computational efficiency.

Model selection was conducted through an iterative optimisation process aimed at identifying the architectures most appropriate of maximizing classification performances for the visual complexity and scale of the dataset.

Each training cycle was guided by performance diagnostics—including learning curve behaviour, loss stability, and validation accuracy—to refine critical hyperparameters such as learning rate, batch size, number of epochs, and the proportion of frozen layers in the pretrained backbone.

To address class imbalance and improve convergence stability, the Asymmetric Loss (ASL Focal Loss) and a Weighted Random Sample (Buda et al., 2018) were applied. A five-fold cross-validation strategy was employed, where the dataset was divided into five subsets. In each iteration, one subset served as the validation set while the remaining four were used for training, providing a balance between model learning and unbiased performance evaluation.

Finaly, the Cosine Annealing Warm Restarts (CAWR) scheduler (Loshchilov and Hutter, 2016) was employed to improve convergence stability and help the model escape suboptimal local minima.

2.2.3. Evaluation and metrics

Classification data were analysed by confusion matrices to oppose predicted values against actual ones. To evaluate the performance of the binary classifications, the Matthews correlation coefficient (MCC) (Matthews, 1975) was selected and calculated as follows:

$$MCC = \frac{TP \times TN - FP \times FN}{\sqrt{(TP + FP) \times (TP + FN) \times (TN + FP) \times (TN + FN)}}$$

Where TP are true positives, TN are true negatives, FP are false positives and FN are false negatives. MCC range is [-1, +1]. The advantages of MCC over other more common metrics, such as accuracy or F1 score, are its invariance for classes imbalance (to which the accuracy is affected) and class swapping (to which F1 is not symmetric) (Chicco and Jurman, 2020, 2023). Furthermore, MCC considers all four classification results (TP, TN, FP and FN) as compared to F1 which does not include TN. Therefore, MCC is also more robust, realistic and less optimistic than F1 score and accuracy.

To further explore model behaviour as recommended by van der Maaten and Hinton (2008), t-distributed Stochastic Neighbour Embedding (t-SNE) was employed to visualize the learned feature representations and highlight clustering patterns. Finally, Gradient-weighted Class Activation Mapping (Grad-CAM) (Selvaraju et al., 2017) was applied to visualize the discriminative regions within input images that contributed most to the model's predictions, thereby enhancing interpretability.

2.2.4. Best model and real-time pipeline

The selected model was ConvNeXt-Tiny, with input images resized to 384 × 384 pixels. Hyperparameters were optimised, and the architecture was enhanced with three Transformer encoder blocks inspired by Vaswani et al. (2017), along with attention pooling modules derived from the Set Transformer approach (Lee et al., 2019) (Details in Supplementary Fig. S1). This design improved the model's ability to capture global interactions and resulted in the best overall performance on the

dataset.

A processing pipeline was developed with practical usability on small embedded devices as a main objective, prioritising speed and ease of deployment. Its purpose is to enable real-time automated analysis of microscope video streams. The pipeline integrates a YOLOv5 object detection module (Jocher et al., 2020) with a ConvNeXt-Atto backbone adapted to include a single Transformer block and using input images resized to 224 pixels.

The architecture's performance was compared with several widely used CNN models, including VGGNet (Simonyan and Zisserman, 2014), ResNet (He et al., 2016), DenseNet (Huang et al., 2017), Inception (Szegedy et al., 2015), and EfficientNet (Tan and Le, 2019), all evaluated under the same parameter constraints.

Compared with traditional detection and image processing methods, YOLOv5 demonstrated superior speed and robustness, particularly in handling overlapping particles, and outperforming simpler OpenCV-based approaches. In addition, YOLOv5 provides direct access to bounding box coordinates and full control over post-processing (Jocher et al., 2020). While newer versions such as YOLOv8 (Jocher et al., 2023) could be considered in future work (particularly if the project requirements evolve toward instance segmentation or pose estimation) they do not offer significant advantages for the current detection-only task. Consequently, YOLOv5 remains the most practical, efficient, and easily controllable solution for the pipeline as implemented.

3. Results

3.1. Classification performance

The performance of the insect recognition models was evaluated using confusion matrices and standard classification metrics, including the MCC, F1-score, and overall accuracy. The results of the binary model distinguishing insects from non-insects are presented in Table 1. Out of a total of 1234 particles, the model correctly identified 970 non-insects and 233 insects, with only 13 false positives and 18 false negatives. These results correspond to a high MCC of 0.922, a F1-score of 0.937, and an overall accuracy of 0.975, indicating excellent discrimination between the two classes.

The performance of the multiclass model distinguishing non-insects, *T. molitor*, and *H. illucens* are detailed in Table 2. Among 983 non-insect particles, 970 were correctly classified, with 12 misclassified as *T. molitor* and 1 as *H. illucens*. For *T. molitor* (150 particles), 135 were correctly identified, with 13 misclassified as non-insects and 2 as *H. illucens*. Finally, for *H. illucens* (101 particles), 95 were correctly classified. Class-specific MCC values ranged from 0.894 to 0.951, F1-scores ranged from 0.906 to 0.955, and the overall accuracy reached 0.972, demonstrating the robustness of the model in a multiclass setting.

Table 1
Confusion matrix and performance parameters related to binary classification in between insect and non-insect.

Predicted class	Actual class	
	Non-insect	Insect
Non-insect	970	13
Insect	18	233
MCC	0.922	
F1-score	0.937	
Accuracy	0.975	

Table 2
Confusion matrix and performance parameters related to multiclass classification in between *T. molitor*, *H. illucens* and non-insect.

Predicted class	Actual class		
	Non-insect	*T. molitor*	*H. illucens*
Non-insect	970	12	1
T. molitor	13	135	2
H. illucens	5	1	95
MCC	0.921	0.894	0.951
MCC global		0.919	
F1-score	0.984	0.906	0.955
F1-score global		0.948	
Accuracy		0.972	

3.2. Classification explicability

The two-dimensional representation of the features extracted by the model using t-SNE are showed in Fig. 2. Each point corresponds to an image projected from the high-dimensional feature space into two dimensions, matching the particles represented in the confusion matrices. The three classes, *T. molitor*, *H. illucens*, and non-insect, form distinct clusters, indicating that the model successfully learned to differentiate between them.

The clear separation between the *H. illucens* cluster, which appears isolated and compact, and the *T. molitor* cluster, demonstrates strong inter-class discrimination. Meanwhile, the more diffuse distribution of the non-insect cluster indicates a wide range of discriminative features, which can be explained by the heterogeneity and diverse origin of the particles belonging to this class. A few intermediate points reveal ambiguous or visually similar particles, likely due to shared textural patterns between *T. molitor* and non-insect structures, the latter occasionally containing non-cuticular insect particles. A small non-insect subcluster was also observed corresponding to fish bone particles.

Grad-CAM saliency maps highlight the image regions that most strongly influenced the model's predictions. The red and yellow areas indicate regions of highest attention. For *H. illucens*, the model focuses

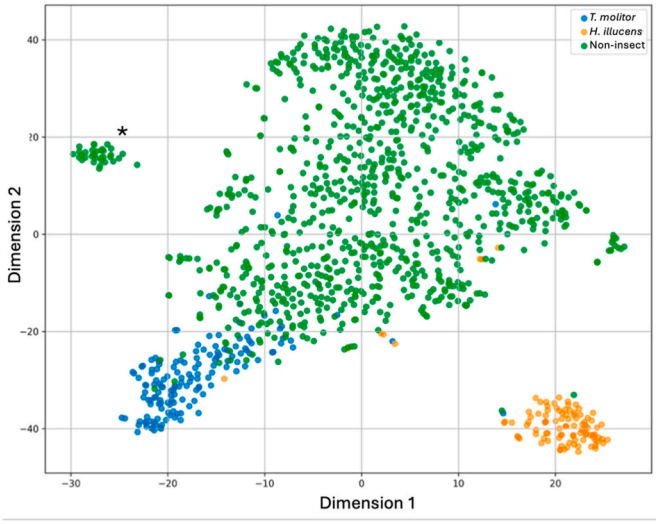

Fig. 2. t-SNE projection of learned features. *T. molitor* samples are shown in blue, *H. illucens* in orange, and *non-insect* samples in green. *, subcluster of fish bone particles.

on characteristic surface structures such as setae and geometric cuticular patterns (Fig. 3). In the case of *T. molitor* and non-insect samples, the activation maps appear more diffuse, suggesting the absence of consistent discriminative features (Fig. 3). Notably, the model accurately identified relevant regions of interest while avoiding artefacts such as air bubbles and non-informative background areas.

3.3. Real-time performance and visualisation

A comparison between the Enhanced Tiny, basic Tiny, and real-time models, as well as other CNN architectures trained under the same protocol and evaluated using identical data splits, is presented in Fig. 4. The models were evaluated according to their average MCC over five folds, the total number of parameters and additionally the training throughput, expressed in frames per second (FPS) (batch size = 16, forward and backward). These measurements were performed on a Google Colab T4 GPU.

The real-time model provides an excellent balance between compactness and performance, achieving an average MCC of 0.85 with only 4.5 million parameters and high training throughput (482 FPS). It clearly outperforms heavier architectures such as ResNet18 (MCC of 0.78, 11.2 million parameters and 511 FPS), DenseNet121 (MCC of 0.79, 7.0 million parameters and 400 FPS), and EfficientNetB2 (MCC of 0.83, 7.7 million parameters and 480 FPS), while maintaining high reliability on the classification task. The Enhanced ConvNeXt Tiny model, although the most complex with nearly 40 million parameters, achieves the best overall performance, with an average MCC of about 0.89, compared to 0.86 for the standard Tiny model with 28 million parameters. This improvement highlights the positive impact of the applied optimisation strategy on model performance for this dataset.

For real-time scenarios, inference performance (batch size = 1) was evaluated on Apple M2 GPU hardware. Table 3 presents comprehensive inference metrics for evaluated real-time architectures. While ResNet18 achieves the fastest inference time (4.42 ms), its lower classification performance (MCC of 0.78, see Fig. 4) makes it less suitable for applications requiring high accuracy. The proposed ConvNeXt-Atto Enhanced model occupies an optimal position in the accuracy-speed-memory trade-off space, achieving competitive inference speed (11.18 ms) with the lowest memory footprint (109 MB) and superior classification accuracy (MCC of 0.85, see Fig. 4).

Each particle detected by the pipeline was highlighted with a bounding box, and the system output included both the predicted class and its associated probability (Fig. 5).

The pipeline was tested on slide images from three types of samples: pure *H. illucens* PAPs, materials of non-insect origin, and a compound feed matrix containing 5% (w/w) *T. molitor*. All analysed particles were smaller than 250 µm.

Results obtained from the pure *H. illucens* slides showed that the model correctly classified between 23% and 30% of the particles as being of insect origin. This outcome can be attributed to the fact that the model was primarily trained to recognise cuticular structures rather than all particle types present in insect meals (e.g., muscular fibres). Consequently, it is expected that not all particles from the insect meal are detected as insect material, as many lack the distinctive morphological features of cuticles.

Samples of non-insect origin were almost entirely classified as non-insect, with only a few particles erroneously identified as insect. However, these false positives exhibited bounding-box probability scores below 60%.

Finally, the analysis of reconstructed images from the compound feed fortified with 5% (w/w) *T. molitor* revealed that approximately 9% of the particles were classified as *T. molitor*, with the remainder identified as non-insect.

4. Discussion

This study demonstrated that insect PAPs can be reliably detected in compound feeds by combining light microscopy with a deep learning approach. Although several alternative techniques for detecting insect PAPs in feed have been developed in recent years, such as PCR (Debode et al., 2017; Marien et al., 2018) or Near Infrared Spectroscopy (Mandrile et al., 2018; Anselmo et al., 2025), the method presented here preserves the advantages of light microscopy while significantly enhancing its detection and identification capabilities at the species level. It is also worth emphasising that light microscopy remains the only official technique for detecting insect PAPs (Veys and Baeten, 2018) and is therefore already routinely used in European control laboratories. Because the approach requires only a standard light

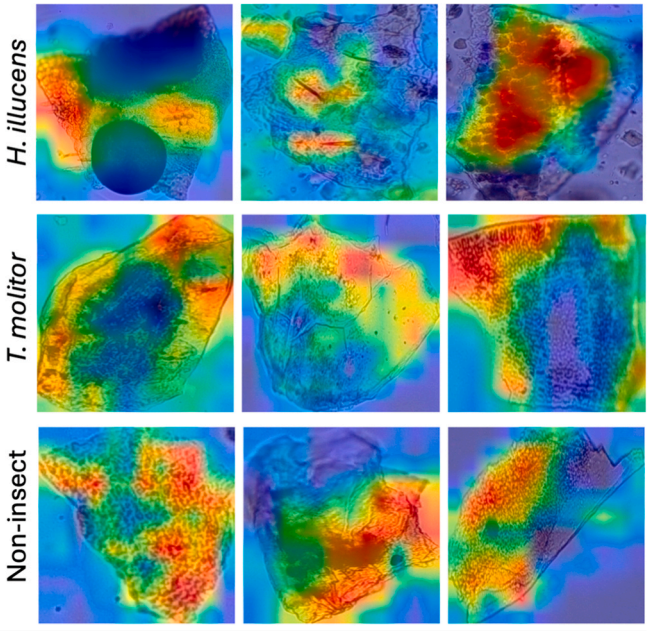

Fig. 3. Grad-CAM visualisation of discriminative regions. Heatmaps generated with Grad-CAM show the particle areas most influential: the closer the colour is red, the higher the influence.

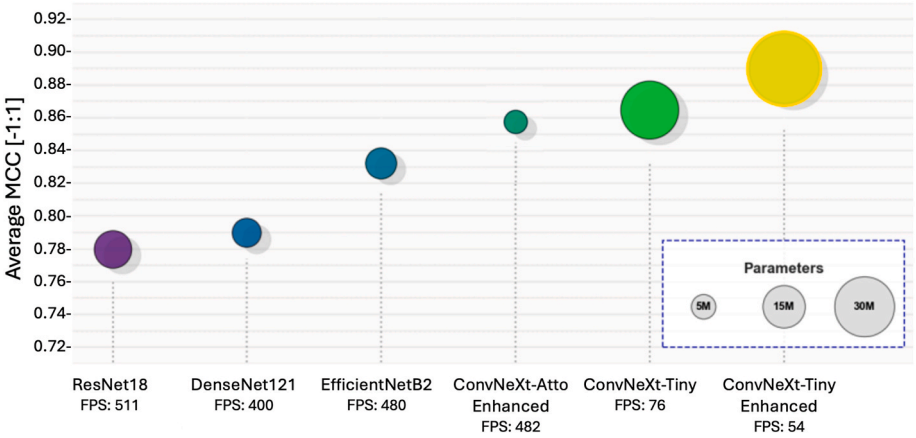

Fig. 4. Comparison of classification performance (MCC) optimised in relation to the number of parameters and lightweight models. FPS: frames per second; M: million parameters.

Table 3
Inference performance comparison on Apple M2 GPU.

Model	Time (ms)	FPS	RAM (MB)
ConvNeXt-Atto Enhanced	11.18 ± 4.24	89.5	109
DenseNet121	16.54 ± 0.33	60.5	283
EfficientNetB2	14.59 ± 3.50	68.5	142
ResNet18	4.42 ± 0.07	226.2	157

microscope and a device capable of running the model and capturing images, it is both accessible and practical for routine implementation.

The proposed model can assist in sample pre-processing and streamline expert evaluation, particularly for samples containing few insect particles, thereby reducing analysis time. It also minimises misclassification by distinguishing visually similar particles, such as wheat aleurone layer cells, which are a common source of analytical error (Veys and Fumière, 2021). Moreover, one slide of the pure insect PAPs slide set from which the model correctly identified 23-30% of particles as *H. illucens* was challenged to three expert microscopists. The same slide, containing approximately 600 insect particles, was analysed by the three experts and the obtained range of insect classification barely reached 15-18%. This small test demonstrated that the model was able to obtain better results than experts could achieve.

The method demonstrated robustness to external variability, as it

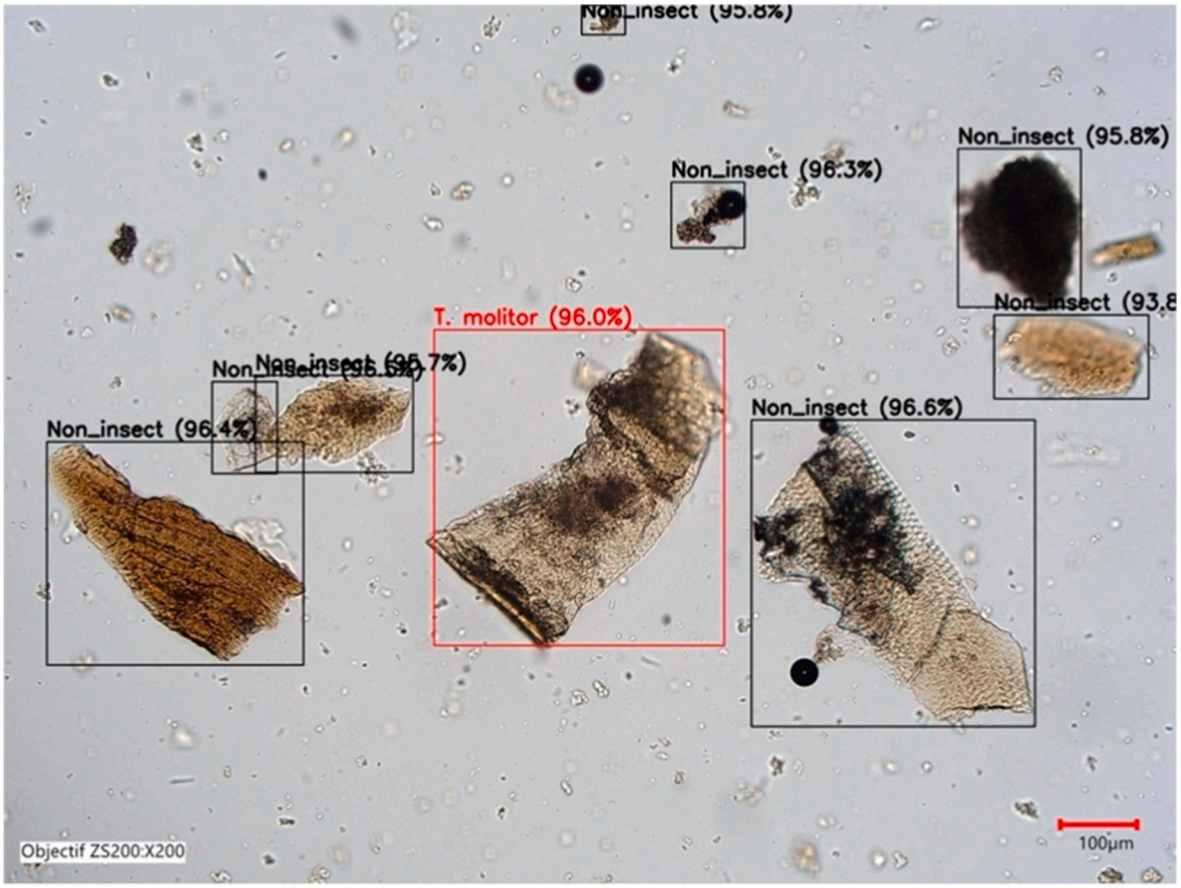

Fig. 5. Illustration of automated model predictions on micrograph obtained with a digital microscope showing bounding boxes and the associated confidence score.

was trained on images acquired from two different microscopes that varied in colour, magnification, and other imaging parameters. This approach enables detailed and interpretable analyses, allowing for particle-level distinction and visual, localised inspection.

Regarding performance, the results indicated that the binary classification model achieves both high accuracy and consistency. The MCC reached values up to 0.92, highlighting the robustness of the classifier even in the presence of class imbalance. Moreover, the model demonstrated a high degree of confidence in predicting the non-insect class, correctly classifying 970 out of 983 samples, corresponding to an accuracy of 0.987. This reflects a conservative prediction strategy that effectively minimises the risk of false-positive insect detections.

In the three-class model, the *H. illucens* class achieved the highest MCC, indicating the most reliable predictions with minimal confusion relative to *T. molitor* or the non-insect class. Some *T. molitor* particles, however, were occasionally misclassified as non-insect. This can be explained by the fact that, within a compound feed matrix, some particles from plant or other feed ingredients may show morphological similarities with *T. molitor* particles which are known to be less differentiated (Ottoboni et al., 2017).

Future work should focus on applying dimensionality reduction techniques, such as UMAP (McInnes et al., 2018), to help reveal ambiguous particle clusters and guide the definition of new intermediate categories (e.g., "non-diagnostic cuticles"). Furthermore, integrating automated microscopy with genomic methods could further reduce ambiguity and enhance the robustness of insect PAP detection.

Importantly, greater attention should also be given to the particle size characteristics used by the model. In this study, no size-based filtering was applied, and particles of all dimensions were analysed together. This lack of size control may have impacted classification performance in several ways. Indeed, very small particles in grinded feed often lack distinctive morphological features (Veys et al., 2017), increasing the likelihood of misclassification. This rules also for very large particles, due to their opacity to the light masking relevant morphological features useful for the operator or the developed AI model. Implementing size-based selection criteria of particles would allow the model to focus more effectively on relevant morphological features, potentially improving classification accuracy (Gonzalez and Woods, 2007)

Finally, the unexpected subcluster observation of the fish bones, as revealed by t-SNE, among the non-insect particles opens interesting perspectives. Although the deep learning model was only parameterised for insect against other particles detection (supervised approach), it was able to isolate fish bones demonstrating its capacity and readiness to classify particles from other animal origin by its learning processing. Therefore, the use of such deep learning model for unsupervised approaches should be investigated.

5. Conclusion

The present research demonstrated the feasibility of applying deep learning to the automated identification of insect particles in compound feeds. The deep learning model proved to be capable of distinguishing insect from non-insect particles with high classification performance, confirming its robustness and its ability to generalise across diverse microscopic conditions. It also demonstrated a capacity to differentiate and identify reliably insect particles at the species level in between *H. illucens* and *T. molitor*, a distinction that remains challenging even for experienced microscopists.

The proposed approach offers several operational advantages: it standardises microscopic analysis, it reduces operator subjectivity and significantly accelerates routine analyses. Its lightweight architecture enables real-time inference on modest hardware, making it accessible to both advanced laboratories and facilities with limited technical resources. The developed proof of concept is a real-time decision-support tool by integration of AI into regulatory microscopy.

Credit author statement

Conceptualization: P. Veys and A. Anselmo; Methodology: C. Kaisin; Software: C. Kaisin; Validation: C. Kaisin; Formal Analysis: C. Kaisin; Resources: A. Anselmo; Data Curation: C. Kaisin and A. Anselmo; Writing – Original Draft: C. Kaisin; Writing – Reviewing & Editing: P. Veys, A. Anselmo and B. Gosselin; Supervision: P. Veys, A. Anselmo and B. Gosselin.

Funding sources

This research did not receive any specific grant from funding agencies in the public, commercial, or not-for-profit sectors.

Declaration of competing interest

The authors declare that they have no known competing financial interests or personal relationships that could have appeared to influence the work reported in this paper.

Acknowledgements

The authors would like to thank Céline Veys and Alexandre Jumet, for microscopic image records for the reference dataset, Alexandra Cordonnier and Lisa Plasman for technical support. This study could not be realised without the support of the International Platform of Insects for Food and Feed (IPIFF).

Appendix A. Supplementary data

Supplementary data to this article can be found online at https://doi.org/10.1016/j.crfs.2026.101374.

References

Anselmo, A., Pissard, A., Vincke, D., Arnould, Q., Lecler, B., Gofflot, S., Michez, D., Baeten, V., 2025. Contribution of vibrational spectroscopy to the characterisation and detection of insect meal in compound feed. Ital. J. Anim. Sci. 24 (1), 763–771. https://doi.org/10.1080/1828051X.2025.2468337.

Bin Zahir Arju, M.Z., Hridi, N.A., Dewan, L., Suhaila, Amin, M.N., Rashid, T.U., Azad, A. K., Rahman, S., Hossain, M., Habib, A., 2025. Deep-learning enabled rapid and low-cost detection of microplastics in consumer products following on-site extraction and image processing. RSC Adv. 15 (14), 10473–10483. https://doi.org/10.1039/d4ra07991d.

Buda, M., Maki, A., Mazurowski, M.A., 2018. A systematic study of the class imbalance problem in convolutional neural networks. Neural Netw. 106, 249–259. https://doi.org/10.1016/j.neunet.2018.07.011.

Chicco, D., Jurman, G., 2020. The advantages of the Matthews correlation coefficient (MCC) over F1 score and accuracy in binary classification evaluation. BMC Genom. 21 (1), 1–13. https://doi.org/10.1186/s12864-019-6413-7.

Chicco, D., Jurman, G., 2023. The Matthews correlation coefficient (MCC) should replace the ROC AUC as the standard metric for assessing binary classification. BioData Min. 16 (1), 1–23. https://doi.org/10.1186/s13040-023-00322-4.

d'Ascoli, S., Touvron, H., Leavitt, M., Morcos, A., Biroli, G., Sagun, L., 2022. ConViT: improving vision transformers with soft convolutional inductive biases. J. Stat. Mech. Theor. Exp. (11), 114005. https://doi.org/10.1088/1742-5468/ac9830, 2022.

Debode, F., Marien, A., Gérard, A., Francis, F., Fumière, P., Berben, G., 2017. Development of real-time PCR tests for the detection of *Tenebrio molitor* in food and feed. Food Addit. Contam. 34 (8), 1421–1426. https://doi.org/10.1080/19440049.2017.1320811.

Dosovitskiy, A., Beyer, L., Kolesnikov, A., Weissenborn, D., Zhai, X., Unterthiner, T., Dehghani, M., Minderer, M., Heigold, G., Gelly, S., Uszkoreit, J., Houlsby, N., 2021. *An image is worth 16x16 word : transformers for image recognition at Scale* (No. arXiv: 2010.11929). https://doi.org/10.48550/arXiv.2010.11929.

European Commission, 2009. Commission regulation (EC) no 152/2009 of 27 January 2009 laying down the methods of sampling and analysis for the official control of feed. Off. J. Eur. Union 36 (L54), 1–130.

European Commission, 2017. Commission Regulation (EU) 2017/893 of 24 May 2017 amending Annexes I and IV to Regulation (EC) no 999/2001 of the European Parliament and of the Council and Annexes X, XIV and XV to Commission Regulation (EU) no 142/2011 as regards the provisions on processed animal protein. Off. J. Eur. Union 2017 (138), 92–116.

European Commission, 2021a. Commission Regulation (EU) 2021/1372 of 17 August 2021 amending Annex IV to Regulation (EC) no 999/2001 of the European

Parliament and of the Council as regards the prohibition to feed non-ruminant farmed animals, other than fur animals, with protein derived from animals. Off. J. Eur. Union L 295, 1–17.
European Commission, 2021b. Commission Regulation (EU) 2021/1925 of 5 November 2021 amending certain Annexes to Regulation (EU) no 142/2011 as regards the requirements for placing on the market of certain insect products and the adaptation of a containment method. Off. J. Eur. Union 1925 (L393), 4–8.
FAO, 2013. Edible Insects: Future Prospects for Food and Feed Security. FAO Forestry Paper).
Gonzalez, R.C., Woods, R.E., 2007. Digital Image Processing, 3. Pearson/Prentice Hall.
Goodfellow, I., Bengio, Y., Courville, A., 2016. Deep Learning. MIT Press.
Guo, J., Han, K., Wu, H., Tang, Y., Chen, X., Wang, Y., Xu, C., 2022. Cmt : convolutional neural networks meet vision transformers. *2022 IEEE/CVF Conference on Computer Vision and Pattern Recognition (CVPR)*, 12165-12175. https://doi.org/10.1109/CVPR52688.2022.01186.
He, K., Zhang, X., Ren, S., Sun, J., 2016. Deep residual learning for image recognition. *2016 IEEE Conference on Computer Vision and Pattern Recognition (CVPR)*, 770-778. https://doi.org/10.1109/CVPR.2016.90.
Huang, G., Liu, Z., Van Der Maaten, L., Weinberger, K.Q., 2017. Densely connected convolutional networks. *2017 IEEE Conference on Computer Vision and Pattern Recognition (CVPR)*, 2261-2269. https://doi.org/10.1109/CVPR.2017.243.
Jocher, G., Chaurasia, A., Qiu, Jing, et al., 2023. *YOLOv8*. Ultralytics. https://github.com/ultralytics/ultralytics.
Jocher, G., Stoken, A., Borovec, J., et al., 2020. *YOLOv5*. Ultralytics. https://github.com/ultralytics/yolov5.
Lee, J., Lee, Y., Kim, J., Kosiorek, A.R., Choi, S., Teh, Y.W., 2019. Set transformer : a framework for attention-based permutation-invariant neural networks. arXiv. https://doi.org/10.48550/arXiv.1810.00825.
Li, K., Zhu, X., Qiao, C., Zhang, L., Gao, W., Wang, Y., 2023. The gray mold spore detection of cucumber based on microscopic image and deep learning. Plant Phenomics 5, 1–13. https://doi.org/10.34133/plantphenomics.0011.
Liu, Z., Lin, Y., Cao, Y., Hu, H., Wei, Y., Zhang, Z., Lin, S., Guo, B., 2021. Swin Transformer : Hierarchical Vision Transformer using Shifted windows. 2021 IEEE/CVF International Conference on Computer Vision (ICCV), pp. 9992–10002. https://doi.org/10.1109/ICCV48922.2021.00986.
Loshchilov, I., Hutter, F., 2016. *SGDR: stochastic gradient descent with warm restarts* (Version 5). arXiv. https://doi.org/10.48550/ARXIV.1608.03983.
Ma, L., Yi, J., Wisuthiphaet, N., Earles, M., Nitin, N., 2023. Accelerating the detection of bacteria in food using artificial intelligence and optical imaging. Appl. Environ. Microbiol. 89 (1). https://doi.org/10.1128/aem.01828-22.
Mandrile, L., Fusaro, I., Amato, G., Marchis, D., Martra, G., Rossi, A.M., 2018. Detection of insect's meal in compound feed by Near Infrared spectral imaging. Food Chem. 267, 240–245. https://doi.org/10.1016/j.foodchem.2018.01.127.
Marien, A., Debode, F., Aerts, C., Ancion, C., Francis, F., Berben, G., 2018. Detection of *Hermetia illucens* by real-time PCR. Journal of Insects as Food and Feed 4 (2), 115–122. https://doi.org/10.3920/JIFF2017.0069.
Matthews, B.W., 1975. Comparison of the predicted and observed secondary structure of T4 phage lysozyme. BBA - Protein Structure 405 (2), 442–451. https://doi.org/10.1016/0005-2795(75)90109-9.
McInnes, L., Healy, J., Melville, J., 2018. UMAP: uniform manifold approximation and projection for dimension reduction. arXiv. https://doi.org/10.48550/ARXIV.1802.03426, Version 3.
Othman, S., Rajesh, N., Hussain, M.A., Abd, N., Mohd, J., 2023. Artificial intelligence-based techniques for adulteration and defect detections in food and agricultural industry: a review. J. Agric. Food Res. 12, 100590. https://doi.org/10.1016/j.jafr.2023.100590.
Ottoboni, M., Tretola, M., Cheli, F., Marchis, D., Veys, P., Baeten, V., Pinotti, L., 2017. Light microscopy with differential staining techniques for the characterisation and discrimination of insects versus marine arthropods processed animal proteins. Food Addit. Contam. 34 (8), 1377–1383. https://doi.org/10.1080/19440049.2016.1278464.
Papa, M.L., Wasit, A., Pecora, J., Bergholz, T.M., Yi, J., 2025. Detection of viable but nonculturable E. coli induced by low-level antimicrobials using AI-Enabled hyperspectral microscopy. J. Food Protect. 88 (1), 100430. https://doi.org/10.1016/j.jfp.2024.100430.
Park, B., Shin, T., Kang, R., Fong, A., McDonogh, B., Yoon, S.C., 2023. Automated segmentation of foodborne bacteria from chicken rinse with hyperspectral microscope imaging and deep learning methods. Comput. Electron. Agric. 208, 107802. https://doi.org/10.1016/j.compag.2023.107802.
Przybył, K., Wawrzyniak, J., Koszela, K., Adamski, F., Gawrysiak-Witulska, M., 2020. Application of deep and machine learning using image analysis to detect fungal contamination of rapeseed. Sensors (Switzerland) 20 (24), 1–11. https://doi.org/10.3390/s20247305.
Rossi, G., Psarianos, M., Ojha, S., Schlüter, O.K., 2025. Review : insects as a novel feed ingredient: processing technologies, quality and safety considerations. Animal 19 (3), 101495. https://doi.org/10.1016/j.animal.2025.101495.
Selvaraju, R.R., Cogswell, M., Das, A., Vedantam, R., Parikh, D., Batra, D., 2017. Grad-CAM : visual explanations from deep networks via gradient-based localization. 2017 IEEE International Conference on Computer Vision (ICCV), pp. 618–626. https://doi.org/10.1109/ICCV.2017.74.
Simonyan, K., Zisserman, A., 2014. *Very deep convolutional networks for large-scale image recognition* (Version 6). arXiv. https://doi.org/10.48550/ARXIV.1409.1556.
Szegedy, C., Liu, Wei, Jia, Yangqing, Sermanet, P., Reed, S., Anguelov, D., Erhan, D., Vanhoucke, V., Rabinovich, A., 2015. Going deeper with convolutions. *2015 IEEE Conference on Computer Vision and Pattern Recognition (CVPR)*, 1-9. https://doi.org/10.1109/CVPR.2015.7298594.
Tan, M., Le, Q.V., 2019. EfficientNet: rethinking model scaling for convolutional neural networks. https://doi.org/10.48550/ARXIV.1905.11946.
van der Maaten, L., Hinton, G., 2008. T-SNE for high-dimensional data visualization. J. Mach. Learn. Res. 9, 2579–2605.
van Raamsdonk, L.W.D., van der Fels-Klerx, H.J., de Jong, J., 2017. New feed ingredients: the insect opportunity. Food Addit. Contam. 34 (8), 1384–1397. https://doi.org/10.1080/19440049.2017.1306883.
Vaswani, A., Shazeer, N., Parmar, N., Uszkoreit, J., Jones, L., Gomez, A.N., Kaiser, L., Polosukhin, I., 2017. *Attention is all you Need* (Version 7). arXiv. https://doi.org/10.48550/ARXIV.1706.03762.
Veys, P., Marien, A., Fumière, O., 2024. Combined microscopy-PCR EURL-AP Proficiency Test 2023 Final Version. Centre wallon de Recherches agronomiques. Retrieved from. https://www.eurl.craw.eu/publications/scientific-reports/.
Veys, P., Planchon, V., Colbert, R., Cruz, C., Frick, G., Ioannou, I., Marchis, D., Nordkvist, E., Paradies-Severin, I., Pohto, A., Weiss, R., Baeten, V., Berben, G., 2017. Collaborative study on the effect of grinding on the detection of bones from processed animal proteins in feed by light microscopy. Food Addit. Contam. 34 (8), 1451–1460. https://doi.org/10.1080/19440049.2017.1312558.
Veys, P., Baeten, V., 2018. Protocol for the isolation of processed animal proteins from insects in feed and their identification by microscopy. Food Control 92, 496–504. https://doi.org/10.1016/j.foodcont.2018.05.028.
Veys, P., Fumière, O., 2021. Implementation study on the detection of insect PAP in feed by double sedimentation method PE/TCE followed by light microscopy identification. Centre wallon de Recherches agronomiques. https://doi.org/10.13140/RG.2.2.19391.23206.
Veys, P., Fumière, O., 2023. 2023 IAG Proficiency Test on Animal Proteins in Feed. Centre wallon de Recherches agronomiques. https://doi.org/10.13140/RG.2.2.17624.06406.
Wada, K., 2021. Labelme : Image Polygonal Annotation Tool. https://github.com/wkentaro/labelme.
Yun, S., Han, D., Chun, S., Oh, S.J., Yoo, Y., Choe, J., 2019. CutMix: regularization strategy to train strong classifiers with localizable features. 2019 IEEE/CVF International Conference on Computer Vision (ICCV), pp. 6022–6031. https://doi.org/10.1109/ICCV.2019.00612.
Zhang, H., Cisse, M., Dauphin, Y.N., Lopez-Paz, D., 2017. Mixup : beyond empirical risk Minimization. arXiv. https://doi.org/10.48550/ARXIV.1710.09412, Version 2.
Zinchuk, V., Grossenbacher-Zinchuk, O., 2020. Machine learning for analysis of microscopy images : a practical guide. Curr. Protoc. Cell Biol. 86 (1), 1–14. https://doi.org/10.1002/cpcb.101.